11-1-2013

A Systematic Study of Radiation-Induced Segregation in Ferritic–Martensitic Alloys

Janelle P. Wharry
Boise State University

Gary S. Was
University of Michigan - Ann Arbor

A Systematic Study of Radiation-Induced Segregation in Ferritic-Martensitic Alloys

Janelle P. Wharry
University of Michigan
Present Address: Boise State University

and

Gary S. Was
University of Michigan

Abstract

A systematic approach to measuring radiation-induced segregation (RIS) was used on four ferritic-martensitic (F-M) alloys: T91, HCM12A, HT9, and a Fe-9Cr model alloy, irradiated with 2.0 MeV protons over a range of doses (1-10 dpa) and temperatures (300-700°C). The experimental conditions are established so as to isolate the dependence of RIS on the experimental parameters: temperature, dose and bulk composition. RIS is measured at prior austenite grain boundaries (PAGBs) using the STEM-EDS technique. Chromium is found to enrich at PAGBs in all conditions with the exception being T91 irradiated to 3 dpa at 700°C. The magnitude of enrichment is small (<2 at%). Minor elements Si, Ni, and Cu also enrich consistently. A bell-shaped temperature dependence of RIS is observed in all elements. The amount of Cr enrichment decreases as a function of increasing bulk Cr concentration. Lastly, it is found that the 9Cr model alloy reaches a steady-state Cr RIS behavior at approximately 7 dpa, while the T91 reaches what may be a steady state near 3 dpa, then the amount of enrichment decreases at 10 dpa.

Keywords: radiation-induced segregation, ferritic-martensitic, proton irradiation

1.0 Introduction

A growing global demand for energy, coupled with the increasing importance of homeland security, has sparked the recent interest in Generation IV nuclear technologies. One of the significant challenges of Generation IV designs, however, is finding suitable materials that will withstand the harsh in-reactor operating conditions. Structural components of Generation IV reactors will be subject to high temperatures, corrosive environments, cyclic loading, and radiation damage up to several hundred displacements per atom (dpa). Ferritic-martensitic (F-M) steels are leading candidates for these applications because of their high strength, resistance to thermal stresses, dimensional stability, and low activation [1], [2].

The F-M steels under consideration are predominantly Fe-Cr alloys containing Cr concentrations ranging from approximately 7at% to 15at%. Chromium and minor alloying elements play a critical role in phase formation in F-M steels [1]. These phases may undergo irradiation-induced changes, which could significantly alter the desirable mechanical properties of the alloy. The Cr-rich ferrite α' phase, for example, is of particular importance because of its potential to embrittle the alloy. Precipitates and carbides that are detrimental to the mechanical properties of the alloy can form when the alloy undergoes highly localized changes in bulk concentration at sinks, a phenomenon known radiation-induced segregation (RIS).

RIS is not well understood in F-M alloys. Studies of RIS in F-M alloys in the early 1980s, were conducted with electron and C^+ ion irradiation at high dose rate and on b.c.c. Fe-Cr model alloys with Cr concentrations in the range 5-13at% Cr and various solute additions [3], [4], [5]. Those studies revealed a variety of Cr RIS behaviors, from Cr enrichment by a magnitude of ~17at%, to Cr depletion by a magnitude of ~4at%. Neutron irradiation experiments on

F-M alloys showed Cr enrichment in both a commercial and model alloy (HT9 and Fe-12CrMoVNb, respectively) [6], [7]. Meanwhile, multiple proton and ion irradiation studies reported Cr depletion in commercial HT9 and F82H, as well as in model Fe-13Cr alloys [8], [9], [10]. The most recent studies on RIS in F-M alloys were completed by Gupta, *et al*. [11] and Lu, *et al*. [12], both in 2006, and by Marquis, *et al*. in 2011 [13], [14]. Gupta, *et al*. reported Cr enrichment in proton-irradiated T91, while Lu, *et al*. reported Cr depletion in Ni^{+} ion-irradiated E911 steel. The Marquis studies observed both Cr enrichment and Cr depletion in Fe^{+} ion-irradiated model alloys. Unfortunately, these few experimental studies were conducted using different alloys, irradiating particles, dose rates, temperatures, and doses such that no two results were conducted under the same conditions [13], [14], [15]. Furthermore, the results of these studies are inconclusive, and have thus far not revealed any apparent trends or patterns in the behavior of RIS.

These inconclusive, and in some cases, contradictory experimental results underscore the need for a systematic study of RIS in F-M alloys. This work was designed to conduct a more orderly approach to determine the dependence of RIS on the experimental parameters of temperature, dose, and alloy composition using 2.0 MeV protons. The experimental conditions for this work were established by keeping two of the irradiation parameters of dose, dose rate and temperature fixed, while varying the third, such that a series of experiments would present the behavior of RIS as a function of a single parameter only. The temperature dependence of RIS was studied over a range from 300°C to 700°C, while the alloy and dose remained fixed at T91 irradiated to 3 dpa. Dose dependence was studied at 1, 3, 7, and 10 dpa, at an irradiation temperature of 400°C, in both alloy T91 and an Fe-9Cr model alloy. Lastly, alloy dependence was studied in T91, HCM12A, HT9, and the Fe-9Cr model alloy, with the irradiation dose and temperature fixed at 3 dpa and 400°C.

This paper will present the experimental results, from which four significant RIS behaviors come to light; a bell-shaped temperature dependence, a change from Cr enrichment to Cr depletion with increasing temperature, a decrease in the amount of Cr enrichment with increasing nominal Cr concentration, and finally, a complex dose evolution of Cr enrichment. Explanations of these behaviors and their implications will be discussed.

2.0 Experiment

Experiments were conducted to measure RIS in four F-M alloys: commercial alloys T91, HCM12A, and HT9, and a high-purity Fe-9Cr model alloy. T91 and the 9Cr model alloy are fully martensitic; both have PAGBs ~11 μm in diameter, and martensite laths ~0.4 μm wide by ~5.5 μm long. Because of its slightly higher Cr content, HCM12A exhibits a two-phase microstructure of martensite laths and δ-ferrite needles, both on the order of 0.9 μm wide and 6.1 μm long. HT9, having the highest Cr content, exhibits a three-phase microstructrue of martensite (laths are 0.4 μm wide and 14.6 μm long), δ-ferrite, and retained austenite. Alloy compositions are provided in Table 1, and heat treatments are given in Table 2. It is important to note that some of the component elements are found in such small concentrations that their x-ray intensities are not sufficiently high to make these elements detectable in the STEM/EDX RIS measurements. Therefore, in Table 1, the element compositions marked with an asterisk are detectable in the STEM/EDX method used throughout this work.

The experimental approach in this work is comprised of two main components: proton irradiations and RIS measurements. Each of these components will be described in greater detail in the following subsections. Statistical certainty and confidence in the RIS measurements are given in the final subsection of the Experimental section.

2.1 Proton Irradiations

The alloys were cut into 1.5 x 1.5 x 20 mm bar specimens by electrical discharge machining (EDM). The specimens were then prepared for irradiation by mechanical polishing followed by electropolishing. Mechanical polishing ensured that the specimens had a flat, planar surface for irradiation, and was done using SiC paper beginning with grit 320 and working up to 4000 grit. Electropolishing was conducted to remove the plastic deformation introduced during mechanical polishing. Specimens were electropolished for 20 seconds in a 90% methanol and 10% perchloric acid solution, at temperatures between -40°C and -50°C, with an applied potential of 35 V between the specimen and a platinum mesh cathode.

Specimens were irradiated with 2.0 MeV protons at the Michigan Ion Beam Laboratory using a General Ionex Tandetron accelerator. Throughout the irradiation, the accelerator beam line was maintained at pressures below 1.3 x 10^{-5} Pa. Samples were mounted onto an irradiation stage, which was attached to, but electrically isolated from, the accelerator beam line. Two stages, both of the same design, were used in these experiments. One stage, made of copper, was used for irradiations up to 500°C, and a second stage made of nickel was used for irradiations above 500°C. In all irradiations up to 600°C, a shim filled with indium was sandwiched between the stage and the samples. The indium, liquid at the irradiation temperatures, provided good thermal contact between the stage and samples so as to increase the efficiency of the heat application or removal. The vapor pressure of indium prevented it from being used at temperatures above 600°C. Thus, for the 700°C irradiation, a 0.2 mm thick graphitic sheet was pressed between the stage and the sample; the malleability of the graphitic sheet allowed for reasonable thermal contact between the stage and sample.

Thermocouples were spot-welded onto the samples and were then used to calibrate a 2D infrared thermal pyrometer. The pyrometer continuously recorded the temperatures of three user-specified areas of interest on each of the irradiated specimens. Temperatures were recorded at a frequency of up to 0.1 Hz throughout the experiment, resulting in about 8600 temperature measurements on each of the areas of interest on each specimen over a 24 hr period. Temperatures were maintained to within ±10°C of the target temperature using a combination of an electrical resistance heater and air cooling loop. A tantalum aperture assembly was mounted above the stage to define the area on the samples that was subjected to irradiation.

Displacement damage was calculated with the Stopping and Range of Ions in Matter (SRIM) 2006™ program [16]. A flux of 2.0 MeV protons perpendicularly incident on the samples produced a fairly uniform damage profile between 5 μm and 15 μm with peak damage at a depth of 19 μm. The damage profile for HT9 is shown in Figure 1. All dose measurements and analyses were performed at a depth halfway to the damage peak, or 9.5 μm from the irradiated surface. This depth was selected because it was sufficiently removed from both surface effects and damage peak effects. Furthermore, its location on a relative flat portion of the damage profile was conducive to post-irradiation TEM sample preparation. At a depth of 9.5 μm, and a beam current density of ~22 μA/cm^2, the damage rate calculated by SRIM was 7.58 x 10^{-4} displacements/nm-ion, which is equivalent to a dose rate of 1.2 x 10^{-5} dpa/sec.

The irradiation dose can be calculated from its direct relationship with the beam current incident on the irradiation stage. The beam current was monitored by collecting the total charge incident upon the stage, using a wire to pass the charge into a charge integrator, then sending the integrated signal to a monitoring computer. This technique for measuring beam current was made possible because the stage and stage chamber are electrically connected to one another, but electrically isolated from the rest of the beam line. The charge integrator arbitrarily assigned one "count" for every μC of charge collected, or 10^6 counts/C. The number of counts recorded by the monitoring computer was then used to determine the irradiation dose, according to the following expression:

$$\frac{counts}{dpa} = \frac{N\left(\frac{at}{cm^3}\right)\cdot q\left(\frac{C}{ion}\right)\cdot Area\left(cm^2\right)\cdot\left(\frac{counts}{C}\right)}{R_D\left(\frac{displacements}{angstrom\cdot ion}\right)},$$

where N is the atomic density, q is the charge per incident ion, R_D is the displacement rate from SRIM, and the *Area* is the irradiation area.

3.2 RIS Measurements

Following irradiation, samples were prepared for TEM investigation. The irradiated bar samples were first mechanically thinned from the back (unirradiated) surface, to 200-400 μm using SiC paper. Next, a diamond wafering saw was used to cut the irradiated area into 1.5 mm x 1.5 mm squares, which were then further back-thinned to ~100 μm with SiC paper. The sample squares were then mounted onto a 3 mm diameter gold ring (0.8 mm inner diameter) using M-Bond. The sample was jet electropolished to remove 9.5 μm of material on the irradiated surface, and then

to perforation from the unirradiated surface. Jet electropolishing was performed at temperatures below -40°C in a solution of 5% perchloric acid, 15% 2-butoxyethanol, and 80% methanol, using a South Bay Technologies single-sided jet electropolisher. This TEM disc preparation method reduced the volume of magnetic F-M material on the TEM disc, which reduced distortion and drift in the TEM images.

Grain boundary RIS measurements were performed on a Philips CM200 field emission gun (FEG) TEM/STEM, equipped with an EDX detector, at Oak Ridge National Laboratory. The microscope was focused to optimize the electron probe at a diameter ≤1.4 nm, full width at one-tenth maximum, using an accelerating voltage of 200 kV and beam current on the order of 1 nA. A Philips Compustage double-tilt specimen holder was used at room temperature, which minimized specimen drift during analysis. This specimen holder has a tilt range of ±30° in each of two perpendicular directions, which provided sufficient range to bring grain boundaries into edge-on alignment with the electron probe.

Only prior austenite grain boundaries (PAGBs) were analyzed for RIS. Since PAGBs tended to be higher-angle boundaries, they were often covered with large carbides. Care was taken to ensure that RIS measurements were at least 20 nm from a carbide. When selecting a PAGB for study, the contrast of the grains adjacent to the boundary was also considered. It was desirable to choose a boundary having low-contrasting grains on both sides, meaning that the grains were not strongly diffracting. A strongly diffracting grain would have increased beam broadening through the thickness of the specimen, which would have greatly reduced the resolution of the RIS profile. For the same reason, it was also desirable to select a PAGB located in a thinner region of the specimen.

Once the PAGB segment to be analyzed was identified, it was aligned edge-on to the incident electron probe. Because of the magnetic nature of the F-M specimens, the maximum magnification at which RIS measurements could be performed was limited to 200,000x. Each line scan was comprised of 41 points spaced 1.5 nm apart, resulting in a 60 nm scan length across a PAGB. All measurements were performed with drift correction.

3.3 RIS Data Collection, Processing, and Error Analysis

Many factors were considered to ensure statistical significance of the RIS measurements. All line scans collected for this work targeted a minimum of 20,000 counts in the Cr peak. This target count level was selected as a result of two competing concerns: minimizing the error and collecting data within a reasonable amount of time. The counting error from 20,000 counts is only 1.4%, and this number of counts could usually be achieved with a collection time of 2.5-3.5 minutes on each point along the scan. Longer collection times would provide better counting statistics but would also risk increased drift and damage to the foil.

For each irradiation condition, RIS was measured across at least two PAGBs, to ensure consistency from boundary to boundary. On each PAGB, at least two line scans were collected to ensure consistency along a given boundary. In total, at least five line scans were collected from each condition. With 41 points in each of 5 line scans on each of 19 alloy/irradiation conditions, the total number of EDX spectra collected exceeded 3800. This paper will present all line scans collected from one condition, to demonstrate the consistency across boundaries and amongst all scans. Then, in all subsequent presentations of results, only the following data will be shown: (1) RIS profiles which are representative of the scans collected from the given conditions, and (2) values for the change in grain boundary concentration, averaged over all scans collected from the given conditions.

3.0 Results and Discussion

Results of the RIS measurements will now be presented and discussed. A general overview of the results will be presented first, along with a demonstration of the consistency amongst scans and across boundaries. The absence of pre-existing segregation will be noted. Then, measurements of the dependence of RIS on experimental parameters will be presented and discussed.

The twelve RIS line scans collected from three PAGBs in the specimen of alloy T91 irradiated to 7 dpa at 400°C are shown in Figure 2. In all scans and on all boundaries, Fe was observed to deplete, while Cr, Si, Ni, and Cu were found to enrich. Within each PAGB, the scans are all self-consistent, having composition profiles of approximately the same shape and size for all segregated elements. Likewise, from PAGB to PAGB, the composition profiles have approximately the same shape and size. This level of self-consistency among all scans and from boundary to

boundary, was observed in all conditions studied. Henceforth, RIS data will be presented as: (1) representative line scans, and (2) the change in the grain boundary composition, averaged over all scans taken at a given condition. Table 3 summarizes the change in grain boundary composition and the associated standard deviation of the mean, for all elements and all conditions studied.

Across all irradiation conditions, only small amounts of enrichment or depletion were observed. In T91, Cr enriched with to a maximum of 1.72 wt% and Fe depleted at most by -2.46 wt%, following irradiation to 3 dpa at 450°C. With one exception, Chromium always enriched and was balanced by Fe depletion; the only exception to this behavior was in T91 irradiated to 3 dpa at 700°C, where Cr depletion and Fe enrichment was observed. Minor elements Si, Ni, Cu, and W, if they segregated at all, were consistently observed to enrich. The dependence of these results on temperature, composition, and dose, will be discussed in greater detail in the following subsections.

It is also relevant to note the absence of pre-existing chemical segregation at PAGBs. Table 3 shows that the as-received grain boundary elemental concentrations were within 0.1% of their matrix values in all four alloys studied, confirming that there was no pre-existing segregation of any element studied. Representative Cr concentration profiles from each as-received alloy lack any concentration gradient, as can be seen in Figure 3.

3.1 Temperature Dependence

Temperature dependence of RIS was studied in alloy T91 irradiated to 3 dpa at temperatures ranging from 300°C to 700°C. Representative RIS profiles from these irradiations are shown in Figure 4. This figure is comprised of one plot for each element studied, such that the temperature dependence of RIS of each element can be easily discerned. Error bars are shown for only one temperature in each plot—typically the temperature at which the most RIS was observed—to avoid clutter and obfuscation. Several interesting behaviors can be gleaned from Figure 4. Small amounts of Cr enrichment and Fe depletion were observed between 300°C and 600°C, but at 700°C the behavior reversed to Cr depletion and Fe enrichment. Minor elements (Si, Ni, Cu) segregated only between 400°C and 500°C. Maximum segregation of all elements was observed at irradiation temperatures between 400°C and 500°C. Finally, the width of the segregation profiles—particularly that of Cr—increased as a function of temperature.

The condition-averaged change in grain boundary composition of all elements are plotted as a function of temperature in Figure 5. From this graph, it is clear that segregation of all elements exhibited a bell-shaped temperature dependence. Chromium enrichment and Fe depletion were maximized at 450°C, while enrichment of the minor elements Si, Ni, and Cu were maximized at 400°C. The bell-shaped temperature dependence can be attributed to point defect mobility. At very low temperatures, defects are immobile and cannot diffuse to sinks, thus severely limiting the amount of segregation. At elevated temperatures, high point defect mobility induces back-diffusion, thus removing concentration gradients. Hence, the greatest amounts of segregation occur at moderate temperatures.

Studying RIS behaviors at the extreme temperatures (i.e. 300°C and 600-700°C) offers insight into the mechanisms driving RIS. At the extreme temperatures, some Cr and Fe RIS persisted, although the change in grain boundary concentration is quite small (absolute values ~0.6 wt%). However, minor element RIS was totally suppressed at 300°C and ≥600°C. This observation suggests that the mechanism of RIS of the minor elements differs than that of Cr and Fe.

One of the most notable behaviors of RIS in F-M alloys is the "crossover" from Cr enrichment to Cr depletion (and also Fe depletion to Fe enrichment) between 600°C and 700°C. This type of behavior has never been reported in any other alloy system, most notably the austenitic alloy system, for which RIS is very well-understood and can be explained by the inverse Kirkendall mechanism [17]. Work by Perks, *et al*. [18], [19] and Allen, *et al*. [17], [20] have shown that the interstitial flux alone can describe RIS in austenitic alloys. They have shown that rate theory models in which Ni diffuses via interstitials faster than does Cr, without the effects of the vacancy flux, can sufficiently induce the Ni enrichment and Cr depletion, which are so consistently measured in austenitic alloys. Diffusion in F-M alloys, however, is a more complicated process. *Ab initio* models [21], [22], [23], [24], [25] have shown that Cr diffuses faster than Fe by both vacancies and interstitials in the bcc Fe-Cr system. These model results suggest that Cr RIS in F-M alloys is the result of two competing fluxes: the vacancy flux, which would cause Cr depletion, and the interstitial flux, which would cause Cr enrichment. Since interstitials diffuse faster than vacancies, it is unsurprising, then, that the interstitial flux would cause RIS at lower temperatures, but at higher temperatures, as vacancy diffusion becomes easier, the vacancy flux begins to contribute to RIS. The result of this would be exactly that observed in the

temperature dependence of Cr RIS: the interstitial flux causing Cr enrichment at lower temperatures, then as the vacancy flux becomes more significant at higher temperatures, the vacancy flux would cause Cr to deplete. The existence of this crossover between Cr enrichment and Cr depletion in the experimental measurements is strong evidence that Cr RIS in F-M alloys can be explained by rate theory, as described in more detail in reference [26].
It is also useful to study the temperature dependence of the full width at half maximum (FWHM) of the Cr RIS profiles and the area under the Cr enrichment peak. Experimental measurements of both of these parameters are shown in Figure 6 as a function of temperature. Not surprisingly, the area under the Cr enrichment peak exhibited a bell-shaped temperature dependence, much like the change in grain boundary concentration of Cr does (see Figure 5). The FWHM of the Cr peak, however, increased as a function of temperature because of back-diffusion at elevated temperatures, which caused the broadening of the Cr concentration gradient.

3.2 Composition Dependence

The composition dependence of RIS was determined using a constant irradiation condition of 3 dpa at 400°C for four alloys: T91, HCM12A, HT9 and the Fe-9Cr model alloy. Representative RIS profiles of Cr, Fe, Ni, and Si from these four alloys are presented in Figure 7, which is comprised of one plot for each element. Nickel and silicon are the only minor elements plotted here because they are the only minor elements detectable in all three commercial alloys. Error bars are shown on only one alloy in each plot. As shown in Figure 7, all four alloys exhibited Cr enrichment and Fe depletion. In addition, both T91 and HT9 exhibited Ni and Si enrichment, while HCM12A showed no enrichment of these elements.

In the commercial alloys, the extent of segregation of Cr and Fe decreased with increasing bulk Cr concentration, as shown in Figure 7. This behavior is attributed to the dependence of interstitial migration energy on bulk Cr concentration, which has been calculated by Terentyev, *et al*. [27]. Terentyev showed via *ab initio* modeling that the migration energy of single SIAs decreased with increasing Cr concentration, from 0.31 eV in pure Fe, to 0.23 eV in Fe-15Cr. Terentyev also calculated that ≥~90% of all SIAs in the bcc Fe-Cr system are <110> Fe-Fe dumbbells. Thus, with increasing bulk Cr concentration, a lower interstitial migration energy would cause larger numbers of Fe interstitials to diffuse toward grain boundaries, and therefore limit the amount of Cr enrichment at that boundary. This trend is illustrated in Figure 8, which plots the change in grain boundary Cr concentration as a function of nominal Cr concentration.

A similar argument could be extended to mobile interstitial clusters. The molecular dynamics simulations of Wong, et al. [23] showed that at temperatures up to ~800°C, diffusivity of di- and tri-interstitial clusters in a bcc Fe-1%Cr matrix is as much as an order of magnitude lower than that in pure bcc Fe. If this trend were to continue for more concentrated Fe-Cr alloys, cluster diffusion toward grain boundaries would be suppressed with increasing bulk Cr concentration. These interstitial clusters were calculated to contain >10%Cr in a bcc Fe-10%Cr alloy [23] when using an Fe-Cr potential that predicts an attractive interaction between Cr and interstitials. Note that in a later work, Wong, et al. [22] demonstrated that this potential is more consistent with ab intio predictions than an alternative potential which predicts a repulsive interaction between Cr and interstitials. Thus, diffusion of interstitial clusters would generate Cr enrichment at grain boundaries. But with increasing bulk Cr concentration, suppressed cluster diffusion would decrease the extent of Cr enrichment.

The one exception to the aforementioned trend is the Fe-9Cr model alloy, which exhibited a change in grain boundary Cr concentration that considerably deviated from the trend line connecting the commercial alloys, shown in Figure 8. The dependencies of point defect migration energy as a function of local composition or lattice strain could affect the extent of Cr RIS, but this idea has not yet been investigated further. The mechanisms for the difference between the model and commercial steels are not understood.

From Figure 7, it can be seen that in T91 and HT9, the change in grain boundary concentration of both Ni and Si increased as a function of the bulk Ni and Si concentration, respectively. However, HCM12A exhibited no segregation of Ni or Si. The change in grain boundary Ni and Si concentration was also analyzed as a function of bulk Cr concentration, as illustrated in Figure 8. The change in grain boundary concentration of both Ni and Si did not appear to exhibit any dependence on bulk Cr concentration. The difference illustrated in Figure 8 between the Cr behavior and the Ni and Si behaviors, further substantiates the argument that the mechanism driving Cr RIS differs from that driving minor element RIS.

3.3 Dose Dependence

Dose dependence of RIS in F-M alloys was studied in both T91 and the Fe-9Cr model alloy at an irradiation temperature of 400°C. Irradiations were conducted to doses of 1, 3, 7, and 10 dpa. Representative RIS profiles from all of these irradiation conditions are presented in Figure 9. The change in grain boundary Cr concentration is shown as a function of irradiation dose in Figure 10.

The alloys exhibited somewhat different dose dependences, most notably at high doses (i.e. ≥ 7 dpa). In the 9Cr model alloy grain boundary Cr increased, from 1 dpa to 7 dpa and appeared to level out or saturate between 7 dpa and 10 dpa. Conversely, Cr enrichment in T91 reached a peak between 3 dpa and 7 dpa and then decreased between 7 dpa and 10 dpa. At all doses, however, Cr enrichment persisted in alloy T91. While the data point for T91 at 10 dpa may appear to be an outlier, this result was the average of fifteen different line scans, from which three scans were taken across each of five different grain boundaries. The five grain boundaries were taken from two different TEM specimens. The standard deviation of the mean at 10 dpa is only 0.25 wt%, which suggests that the set of fifteen line scans is self-consistent. As can be seen in Figure 9, these minor elements enriched at all doses in alloy T91, but the change in their grain boundary concentration increased from 1 dpa to ~3-7 dpa, then decreased from ~3-7 dpa to 10 dpa.

Differences in composition between T91 and 9Cr model alloy may explain the difference in the dose dependence of Cr and Fe RIS between these two alloys. While the 9Cr model alloy is almost totally free of minor elements and impurities, the results presented in this paper have shown that minor elements Ni, Si, and Cu enriched consistently in alloy T91—often to 3-4 times their bulk levels. Such considerable enrichment of these minor elements in T91 could induce local composition effects, particularly in the vicinity of the grain boundary where Ni, Si, and Cu are found to be enriched. As shown in Table 4, Si [31], Ni [32], and Cu [33] all have atomic radii smaller than that of Cr [34] and Fe [35]. The increased concentration of Ni, Si, and Cu at the grain boundary could decrease the lattice parameter in the immediate vicinity of the grain boundary. It would then follow that Cr atoms would become less undersized and the migration energy of Cr would increase locally, causing a reduction in the amount of Cr enrichment.

Another possible explanation for the reduction in Cr enrichment between 7 dpa and 10 dpa, could be back diffusion and the broadening of the concentration gradients. Figure 11 shows that the FWHM of the Cr enrichment peak increased with dose, especially between 7 dpa and 10 dpa. Furthermore, the area under the Cr enrichment peak—or, the total amount of Cr segregated to the grain boundary—remained constant between 7 dpa and 10 dpa. Together, these measurements show that the total *amount* of Cr segregated at the boundary reached a steady state, even when the change in grain boundary Cr concentration did not demonstrate a steady state. Segregated Cr has redistributed itself in the vicinity of the grain boundary, perhaps when it became energetically favorable to do so due to local composition effects.

3.4 Literature Data in the Context of this Work

The purpose of this study was to clarify the behavior of RIS in F-M alloys using a systematic approach, given that earlier experiments in the literature appeared to be absent of any remarkable trends or consistencies. But it is now relevant to consider the literature data in the context of the RIS behaviors found in this study, and identify any similarities. In this section, the temperature and alloy dependencies of Cr RIS from literature will be compared to those dependencies measured in this work.

The temperature dependence is examined first. Electron irradiation experiments are excluded from the survey of literature on Cr RIS in F-M alloys, because the damage cascade efficiency of electron irradiations is considerably greater than that of neutrons, protons, and heavy ions [36]. From the remaining literature, the reported values of the change in grain boundary Cr concentration (wt%) are shown as a function of temperature in Figure 12. Note that in this figure, the open squares are data from studies in which only the direction—not the magnitude—of Cr RIS was reported, so an arbitrary value is plotted in Figure 12 for the purpose of illustrating the direction of RIS.

It is clear from Figure 12 that at moderate temperatures (~350-500°C), only Cr enrichment was reported in literature. The majority of instances of Cr depletion occurred only at very high temperatures (≥500°C); this is consistent with the temperature dependence measured in this work, in which Cr enrichment switched to Cr depletion with increasing temperature. However, there were three instances of Cr depletion at lower temperatures (250°C [10] and 300°C [12]),

which is inconsistent with the results of this work. These instances of Cr depletion at lower temperatures were collected under differing experimental parameters (e.g. dose, damage rate, alloy) and using differing experimental techniques (e.g. specimen geometry, examination depth relative to ion implantation depth, type of boundary examined). Thus, without systematically evaluating how each of these parameters and techniques affects Cr RIS, it remains difficult to identify consistency between the scattered literature data and the results of this work.

Even with respect to the alloy dependence of Cr RIS, the non-systematic data from literature is difficult to interpret in the context of this work. Electron and non-alloying element ion irradiation experiments are excluded from the survey of literature on Cr RIS in F-M alloys; the ion irradiation experiments that used non-alloying element ions (e.g. C^+ ions to irradiate a high-purity Fe-13Cr) are excluded here because of the potential precipitation and microchemical effects of implanted impurity elements. The remaining Cr enrichment data reported in literature are then plotted as a function of bulk Cr concentration in Figure 13. In this figure, there may be a tendency for Cr depletion to occur at higher bulk Cr concentrations (≥12 wt%), which is the direction measured in this work in which a decreasing amount of Cr enrichment occurred with increasing bulk Cr concentration. However, Cr depletion was also observed at <8 wt% bulk Cr, and considerable magnitudes of Cr enrichment are observed in alloys containing ≥12 wt% Cr. There is again significant variability in experimental parameters and techniques of the literature data, thus making it difficult to determine consistency between literature and this work. The study presented in this paper, in which experimental parameters are well-controlled and systematically varied, demonstrates the value of a systematic approach, from which trends can be more easily identified and comparisons to other systematic studies can be more effectively drawn.

4.0 Conclusions

Radiation induced segregation in F-M alloys was systematically measured to determine the dependence of RIS on temperature, bulk concentration, and dose. The results can be summarized as follows:

- In all four alloys (T91, HCM12A HT9 and model Fe-9Cr), Cr enriched at PAGBs over the temperature range300°C to 600°C, and the dose range 1-10 dpa. The *only* exception to this observation occurred in T91 irradiated to 3 dpa at 700°C, where Cr depleted.

- The temperature dependence of Cr and Fe RIS followed a bell-shaped curve. The temperature dependence of minor element (Ni, Si, Cu) RIS also followed a bell-shaped curve, but the temperature range over which they segregated was more limited (400-500°C) than that over which Cr and Fe segregated (300-700°C), suggesting that the driving mechanism of minor element RIS differed from that of Cr RIS.

- A "crossover" between Cr enrichment and Cr depletion was observed between 600°C and 700°C in T91 irradiated to 3 dpa. This crossover can be explained by the competition between the interstitial flux and vacancy flux, in which Cr diffuses faster than Fe.

- Chromium enrichment decreased as a function of increasing bulk Cr concentration in the commercial F-M alloys. However, this trend did not hold for the Fe-9Cr model alloy, likely because of the absence of minor and impurity elements in the model alloy.

- In the model alloy, Cr RIS reached steady state by ~7-10 dpa. In T91, Cr RIS exhibited a peak at 7 dpa, then decreased at higher doses. It is believed that minor elements affect the dose evolution of RIS, particularly in the commercial alloys.

Acknowledgements

The authors acknowledge O. Toader and F. Naab of the Michigan Ion Beam Laboratory for their assistance with irradiations, and C. Parish, J. Bentley, and J. Busby of Oak Ridge National Laboratory for their assistance with microscopy. Research funded by the DOE Office of Nuclear Energy's Nuclear Energy University Programs under awards DE-FG07-07ID14828 and DE-FG07-07ID14894. Research supported by ORNL's Shared Research Equipment (ShaRE) User Program, which is sponsored by the Office of Basic Energy Sciences, the U.S. Department of Energy.

Tables & Figures

Table 1. Alloy compositions (wt%), compositions marked with an asterisk (*) are detectable in the STEM/EDX setup used in this work.

Alloy / Element	T91	HCM12A	HT9	9Cr Model
Fe	89.15 *	84.22 *	84.92 *	90.9 *
Cr	8.37 *	10.83 *	11.63 *	9.0 *
Mo	0.9	0.3	1	--
Mn	0.45	0.64	0.52	--
Ni	0.21 *	0.39 *	0.5 *	--
V	0.216	0.19	0.3	--
Cu	0.17 *	1.02 *	0.04	--
W	--	1.89 *	0.52	--
Si	0.28 *	0.27 *	0.22 *	--
Nb	0.076	0.054	--	--
C	0.1	0.11	0.2	0.1
N	0.048	0.063	0.047	--
Al	0.022	0.001	<0.01	--
P	0.009	0.016	0.02	--
S	0.003	0.002	0.006	--

Table 2. Heat treatment of alloys studied.

	Austenitizing			Tempering		
Alloy	Temp. (°C)	Time (min)	Cooling	Temp. (°C)	Time (min)	Cooling
T91	1066	46	air	790	42	air
HCM12A	1050	60	air	770	45	air
HT9	1040	30	air	760	60	air
9Cr Model	950	60	air	750	60	air

Table 3. Average change in grain boundary concentration and the standard deviation of the mean, of all elements in all conditions studied.

Sample Designation	Average change in grain boundary concentration (wt%)						Standard deviation of the mean (wt%)					
	Si	Cr	Fe	Ni	Cu	W	Si	Cr	Fe	Ni	Cu	W
T91, As-received	0.00	0.00	0.00	0.00	0.00	N.D.	0.01	0.03	0.04	0.01	0.01	N.D.
T91, 3dpa,, 300C	0.00	0.62	-0.63	0.02	0.00	N.D.	0.02	0.15	0.14	0.01	0.01	N.D.
T91, 1dpa, 400C	0.18	0.74	-1.33	0.25	0.15	N.D.	0.01	0.18	0.18	0.01	0.01	N.D.
T91, 3dpa, 400C	0.28	1.49	-2.28	0.37	0.12	N.D.	0.06	0.19	0.40	0.12	0.05	N.D.
T91, 7dpa, 400C	0.22	1.62	-2.37	0.30	0.21	N.D.	0.02	0.32	0.35	0.05	0.04	N.D.
T91, 10dpa, 400C	0.16	0.87	-0.96	0.20	0.07	N.D.	0.04	0.25	0.26	0.06	0.03	N.D.
T91, 3dpa, 450C	0.23	1.72	-2.46	0.30	0.18	N.D.	0.01	0.04	0.05	0.01	0.01	N.D.
T91, 3dpa, 500C	0.22	1.35	-1.90	0.27	0.02	N.D.	0.04	0.13	0.13	0.03	0.02	N.D.
T91, 3dpa, 600C	0.00	0.64	-0.77	0.01	0.00	N.D.	0.02	0.17	0.28	0.01	0.01	N.D.
T91, 3dpa, 700C	0.02	-0.43	0.41	0.00	0.01	N.D.	0.04	0.12	0.15	0.02	0.01	N.D.
9Cr, As-received	N.D.	-0.01	0.01	N.D.	N.D.	N.D.	N.D.	0.02	0.02	N.D.	N.D.	N.D.
9Cr, 1dpa, 400C	N.D.	0.61	-0.61	N.D.	N.D.	N.D.	N.D.	0.28	0.28	N.D.	N.D.	N.D.
9Cr, 3dpa, 400C	N.D.	0.78	-0.78	N.D.	N.D.	N.D.	N.D.	0.05	0.05	N.D.	N.D.	N.D.
9Cr, 7dpa, 400C	N.D.	1.43	-1.43	N.D.	N.D.	N.D.	N.D.	0.14	0.14	N.D.	N.D.	N.D.
9Cr, 10dpa, 400C	N.D.	1.54	-1.54	N.D.	N.D.	N.D.	N.D.	0.20	0.20	N.D.	N.D.	N.D.
HT9, As-received	0.00	0.01	-0.01	-0.03	N.D.	N.D.	0.01	0.04	0.04	0.03	N.D.	N.D.
HT9, 3dpa, 400C	0.04	0.69	-1.30	0.59	N.D.	N.D.	0.01	0.07	0.07	0.05	N.D.	N.D.
HCM12A, As-received	-0.01	0.07	-0.10	N.D.	-0.03	0.03	0.04	0.03	0.05	N.D.	0.04	0.13
HCM12A, 3dpa, 400C	0.04	0.86	-1.98	N.D.	0.16	0.12	0.81	0.03	0.23	N.D.	0.08	0.69

N.D. = element is not detectable

Table 4. Atomic radii of constituent elements of alloy T91.

Element	Calculated atomic radius (pm)	Empirical atomic radius (pm)
Fe	156 [35]	140 [35]
Cr	166 [34]	140 [34]
Si	111 [31]	110 [31]
Ni	149 [32]	135 [32]
Cu	145 [33]	135 [33]

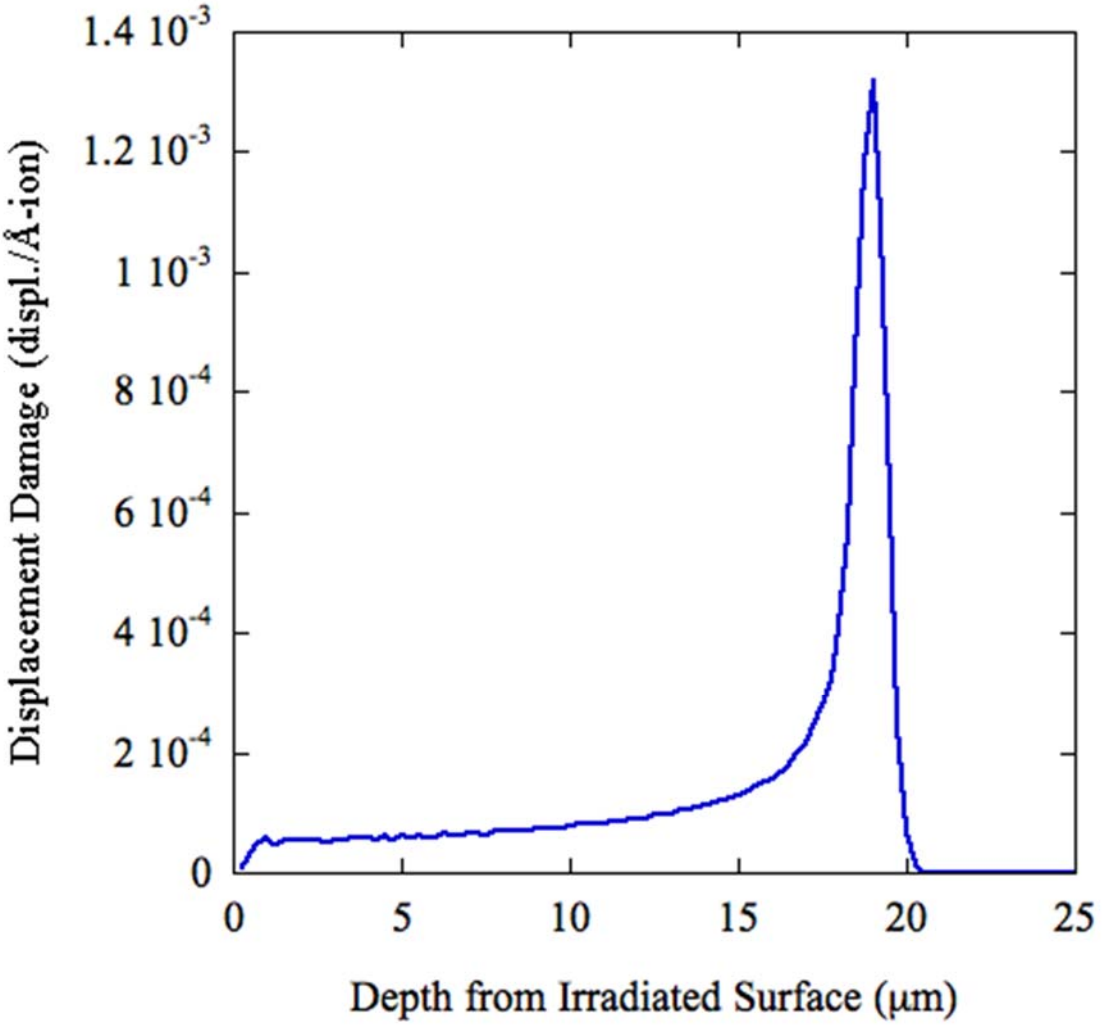

Figure 1. SRIM calculated damage profile for 2.0 MeV protons perpendicularly incident on HT9.

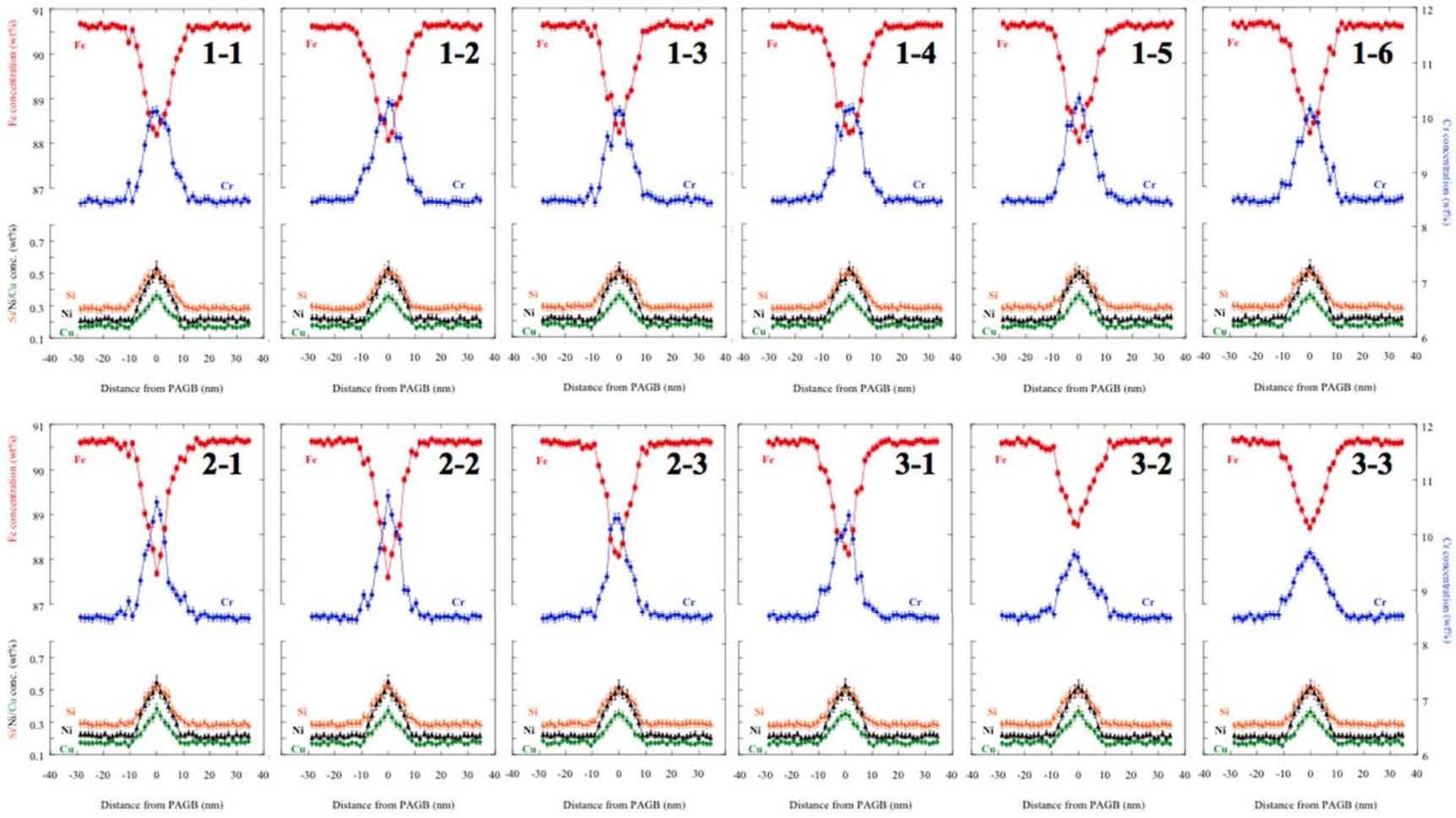

Figure 2. All RIS profiles collected from a specimen of T91 irradiated to 7 dpa at 400°C, '*x*-*y*' indicated on each plot represents the PAGB number (*x*) and scan number on the given PAGB (*y*).

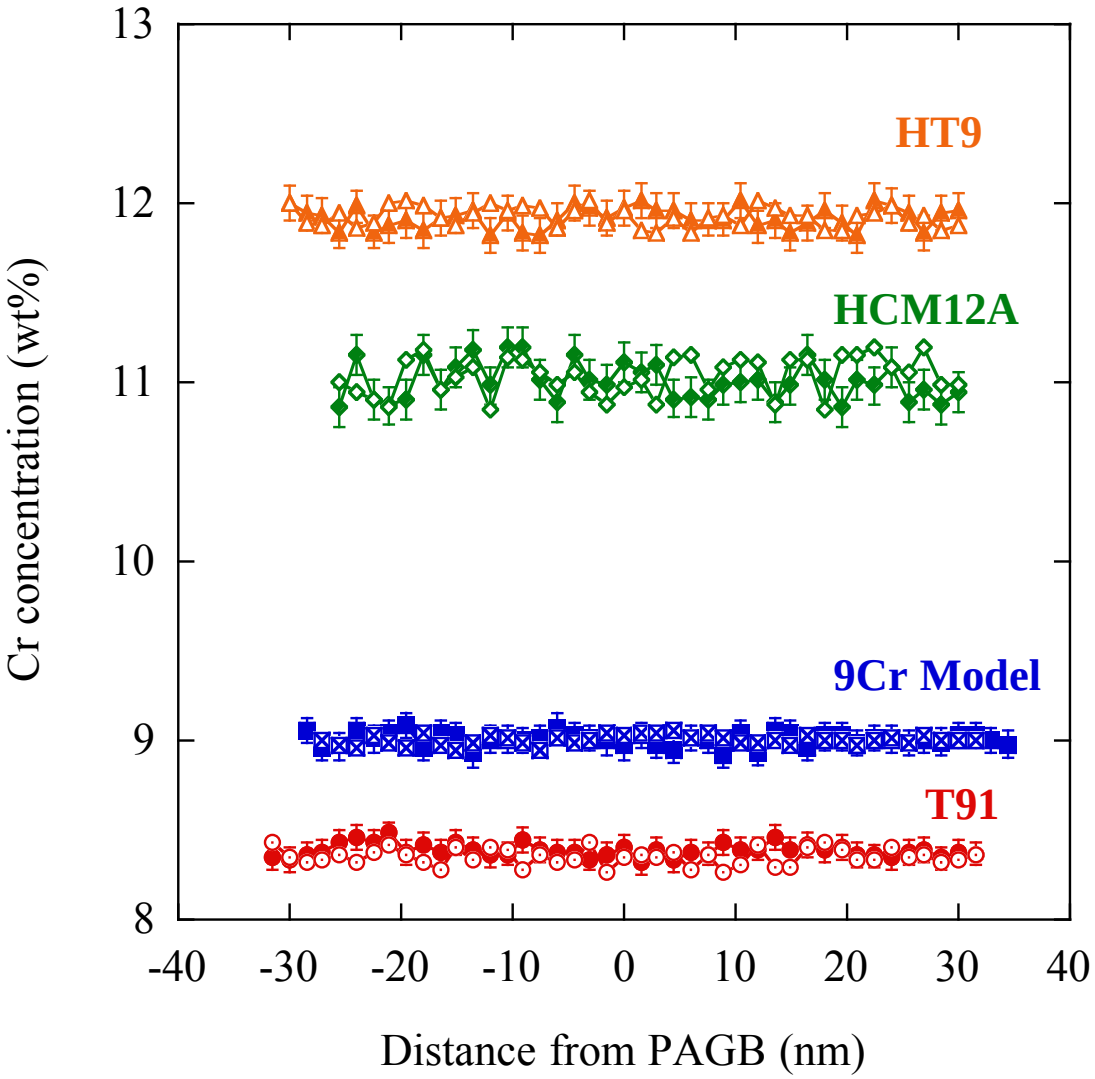

Figure 3. Cr concentrations from two line scans collected in each of the as-received alloys, showing the absence of pre-existing segregation.

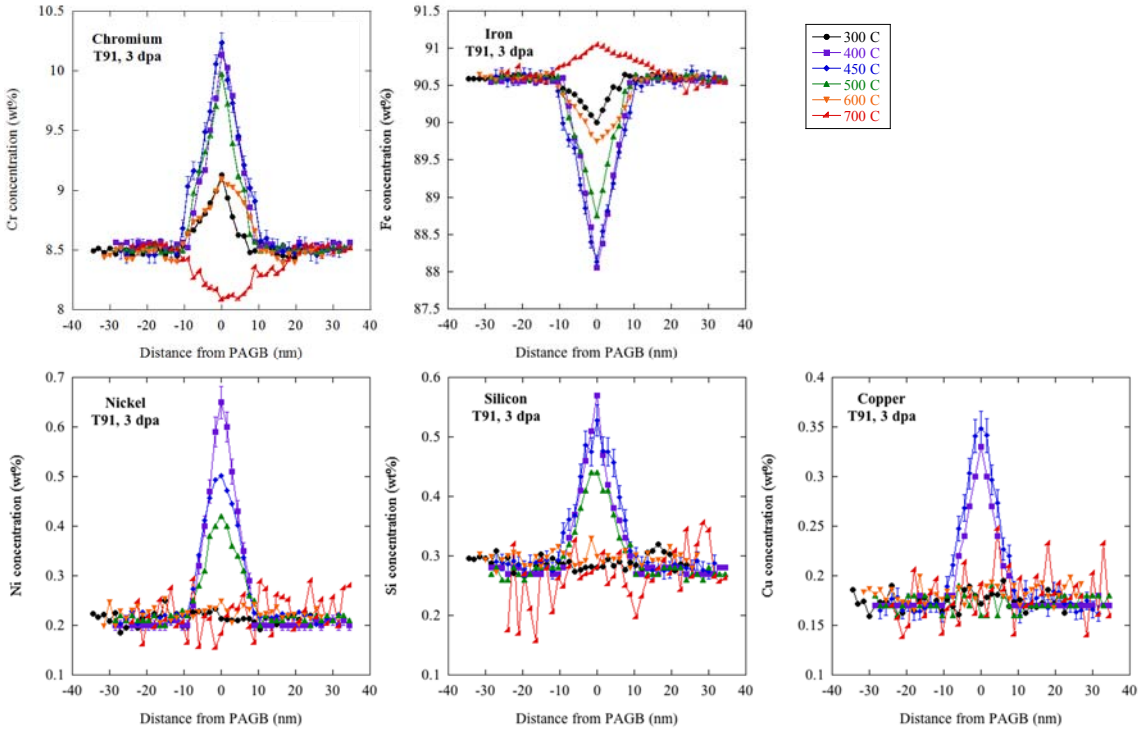

Figure 4. Representative RIS profiles of Cr, Fe, Ni, Si, and Cu, from T91 irradiated to 3 dpa with 2.0 MeV protons, demonstrating temperature dependence.

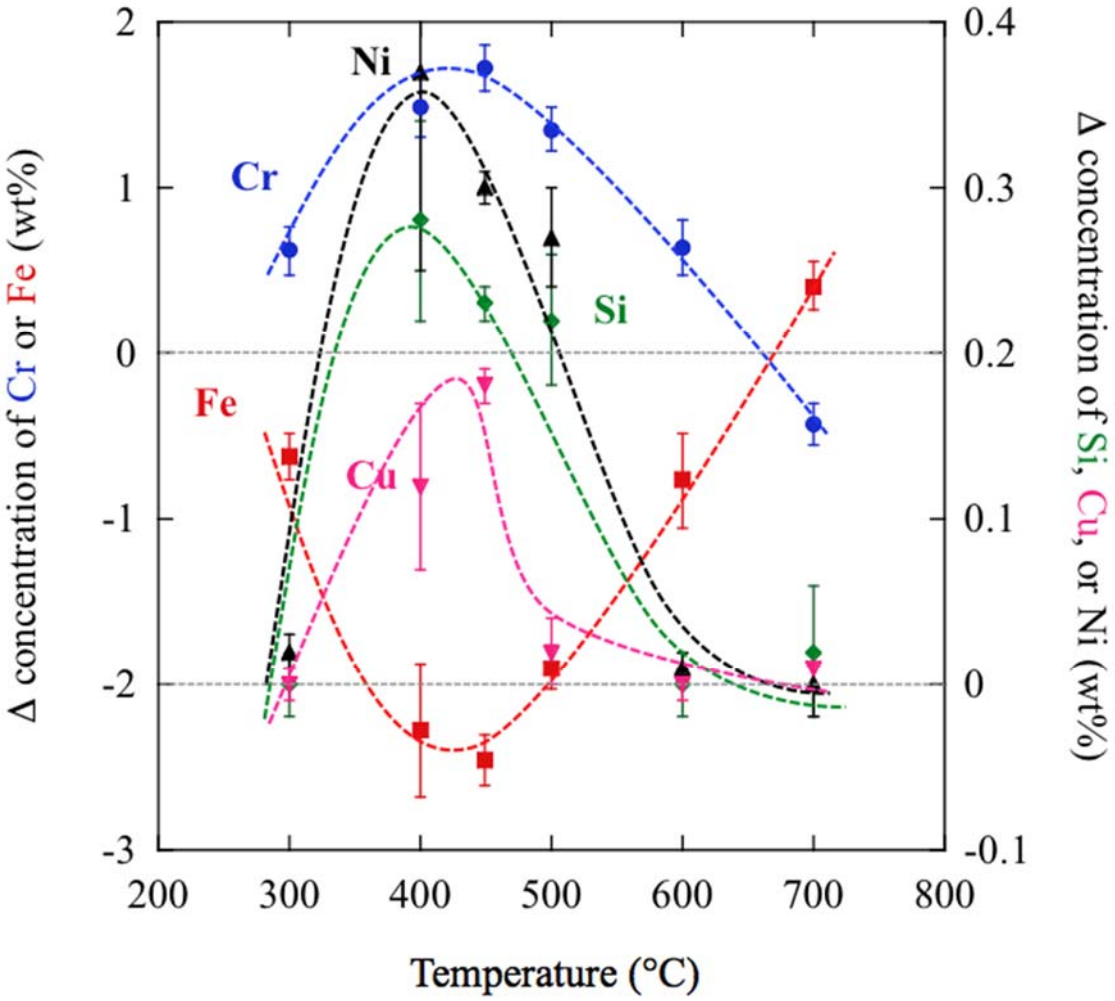

Figure 5. Average amounts of RIS for all elements as a function of temperature, in T91 irradiated to 3 dpa with 2.0 MeV protons.

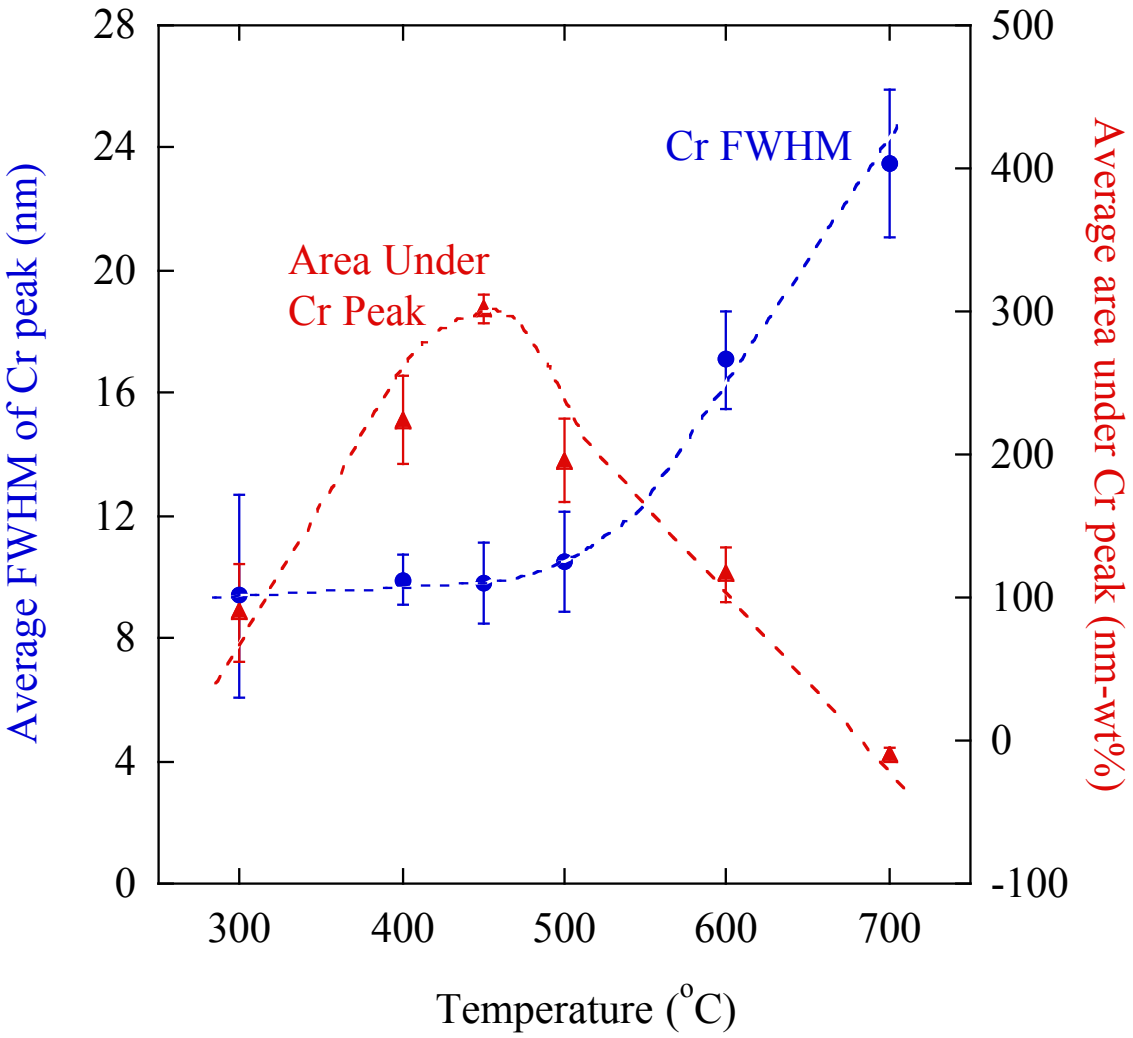

Figure 6. Average FWHM of peak and area under Cr RIS peak as a function of temperature, in T91 irradiated to 3 dpa with 2.0 MeV protons.

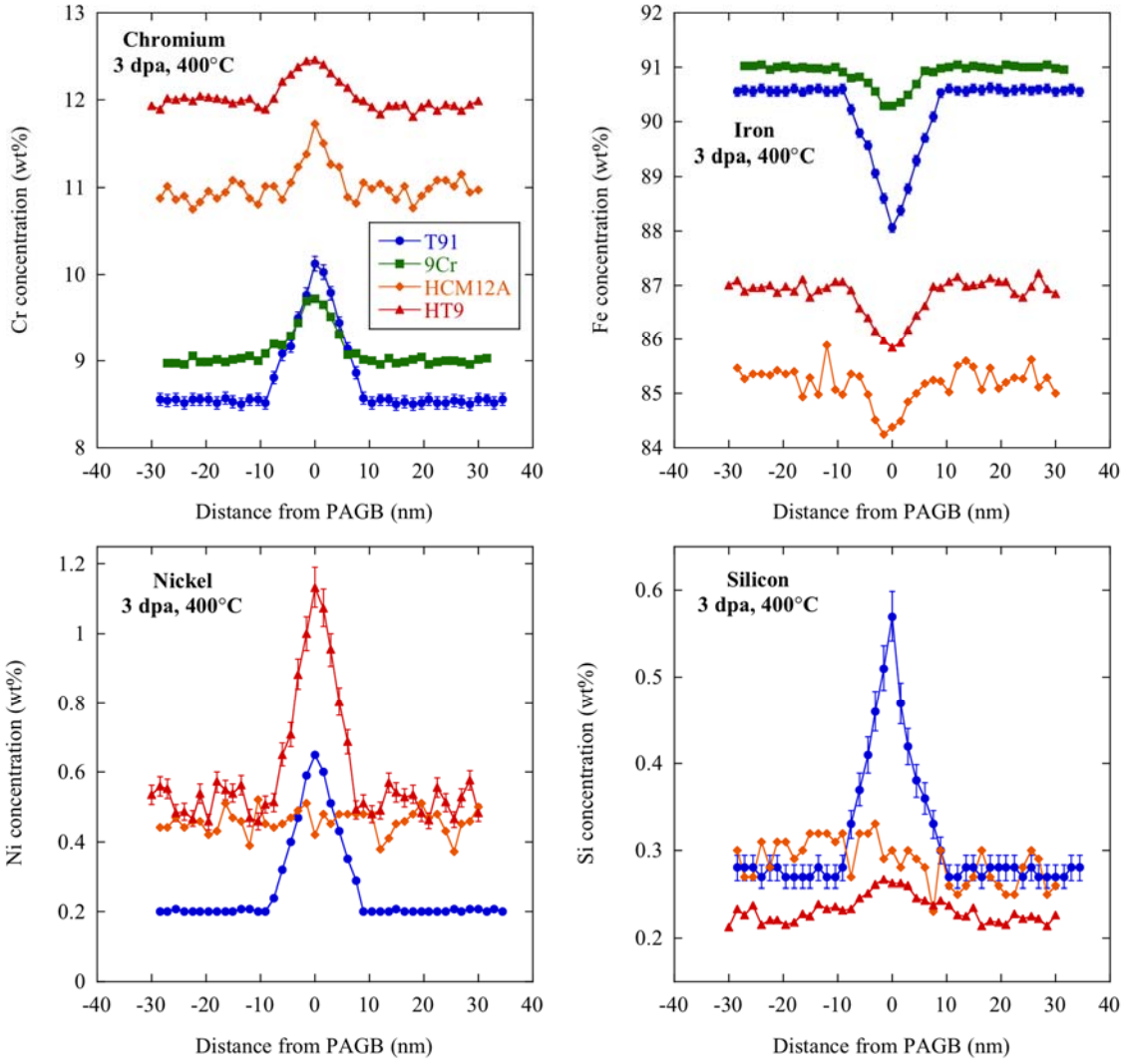

Figure 7. Representative RIS profiles from alloys irradiated to 3 dpa at 400°C with 2.0 MeV protons, demonstrating alloy dependence.

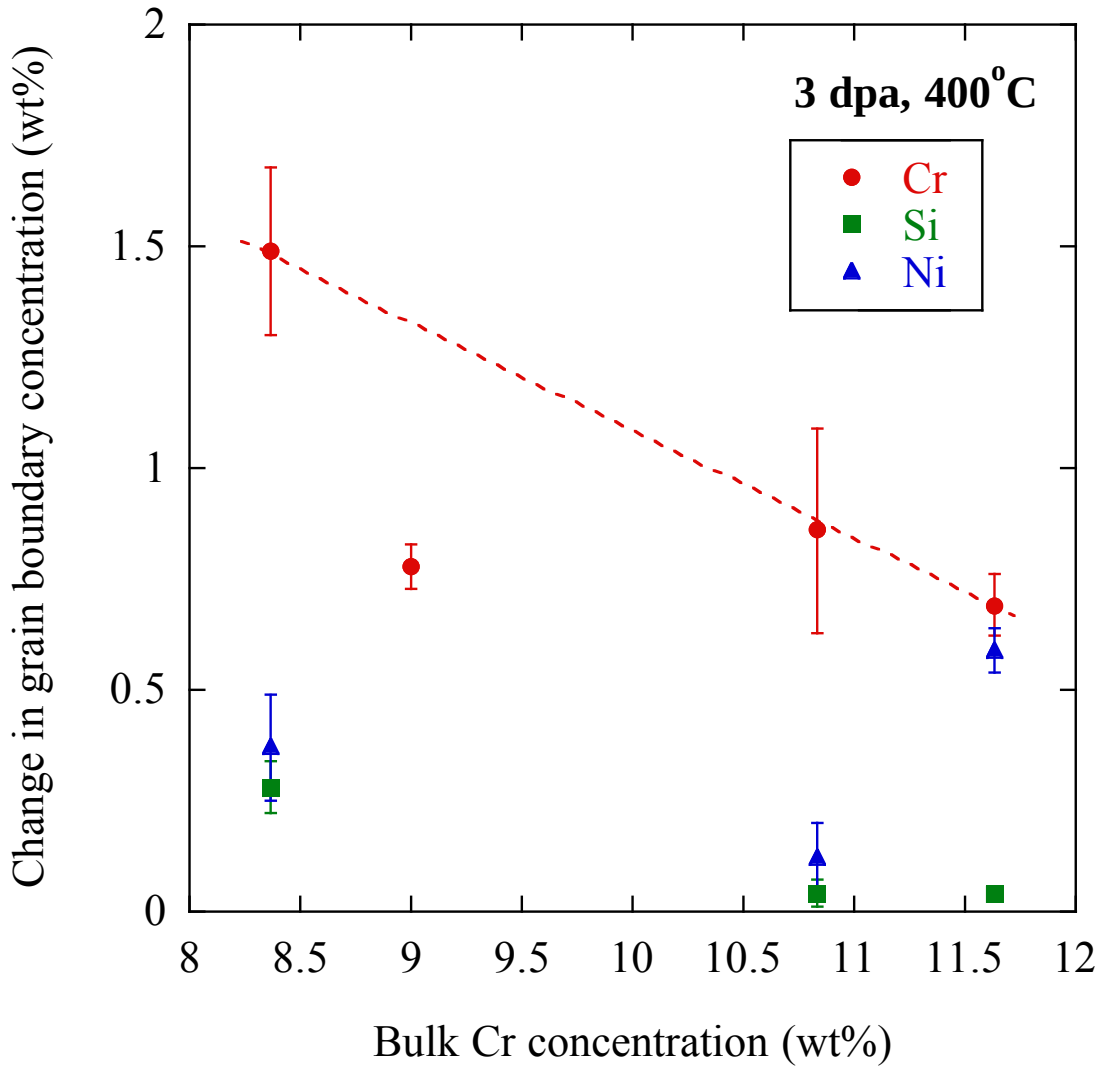

Figure 8. Average change in grain boundary concentration (wt%) of Cr, Si, and Ni in four F-M alloys as a function of bulk Cr concentration, all irradiated to 3 dpa at 400°C with 2.0 MeV protons.

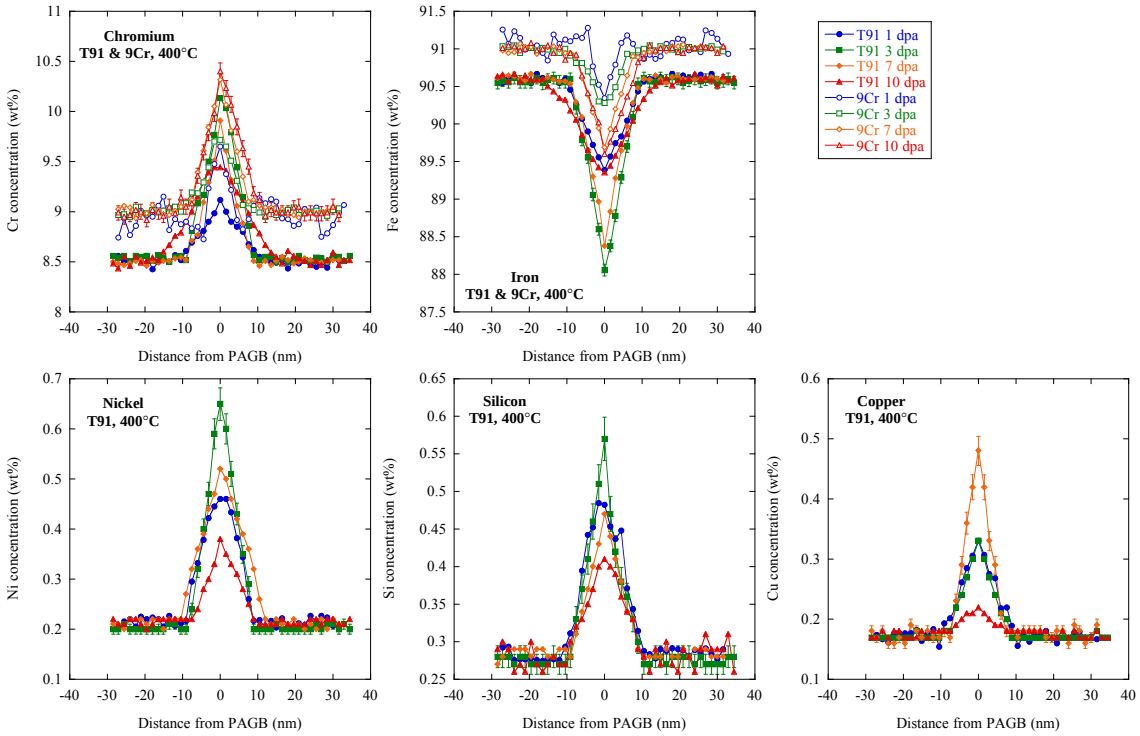

Figure 9. Representative RIS profiles from T91 and 9Cr model alloy irradiated at 400°C with 2.0 MeV protons, demonstrating dose dependence.

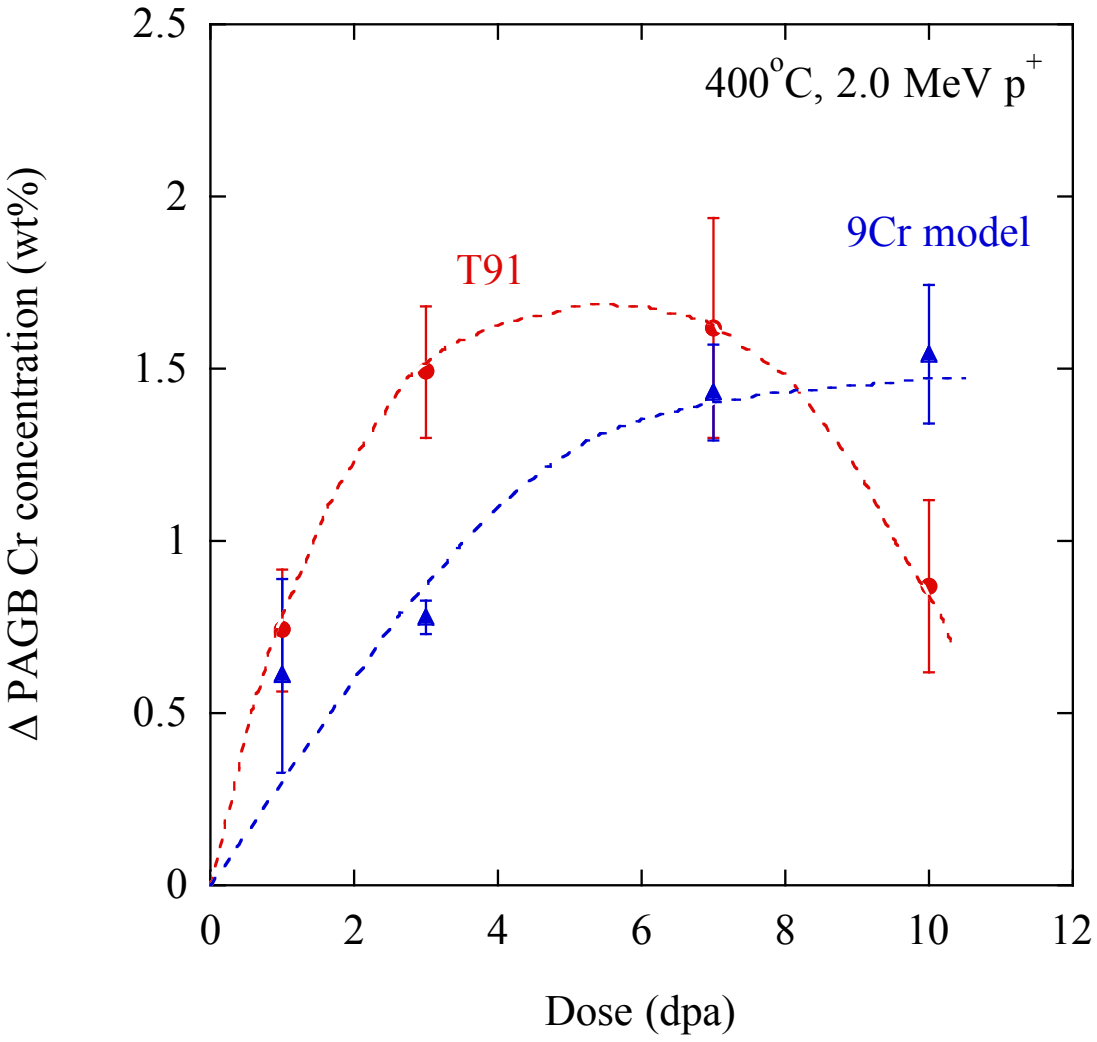

Figure 10. Average amount of Cr RIS in T91 and 9Cr model alloy, as a function of dose, all irradiated at 400°C with 2.0 MeV protons.

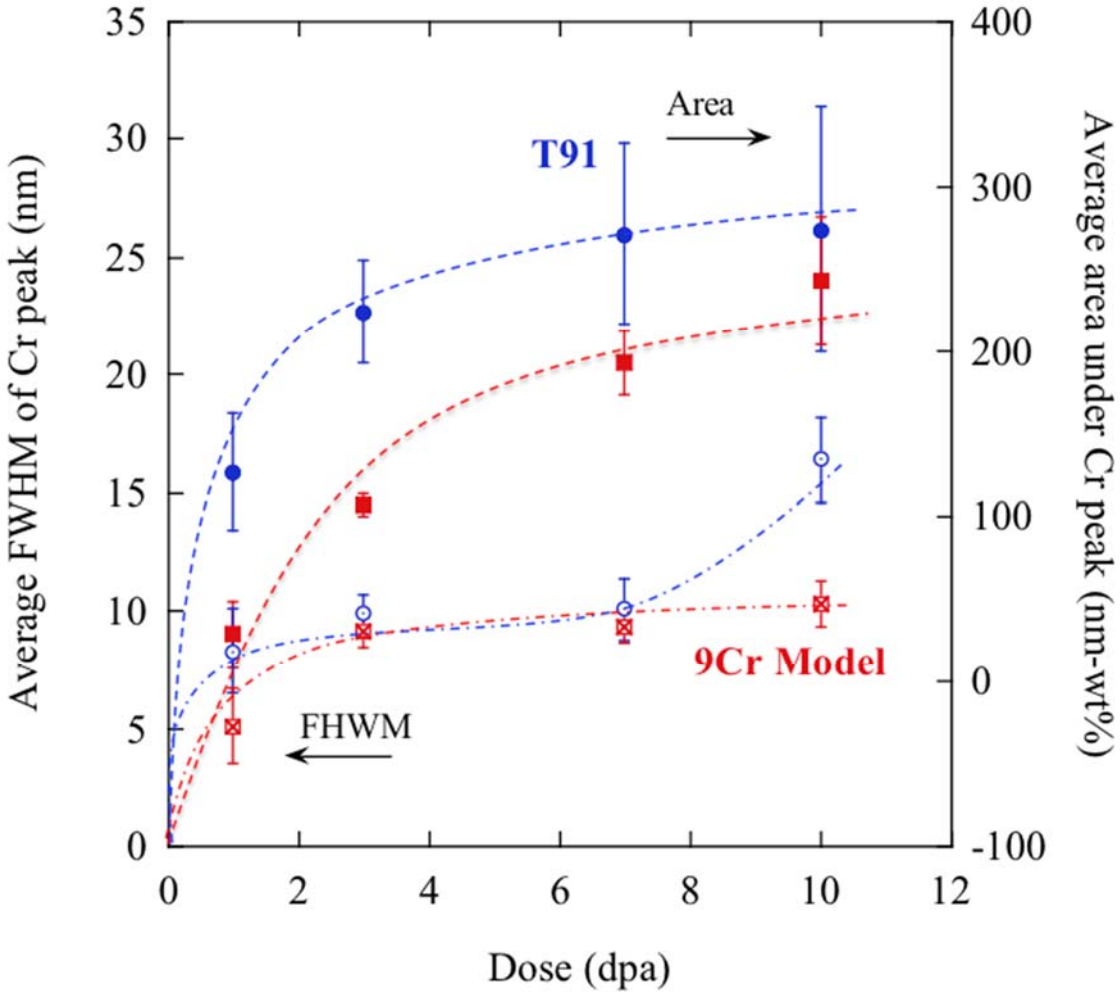

Figure 11. FWHM and area under Cr enrichment peak in T91 and 9Cr model alloy, as a function of dose, irradiated at 400°C with 2.0 MeV protons.

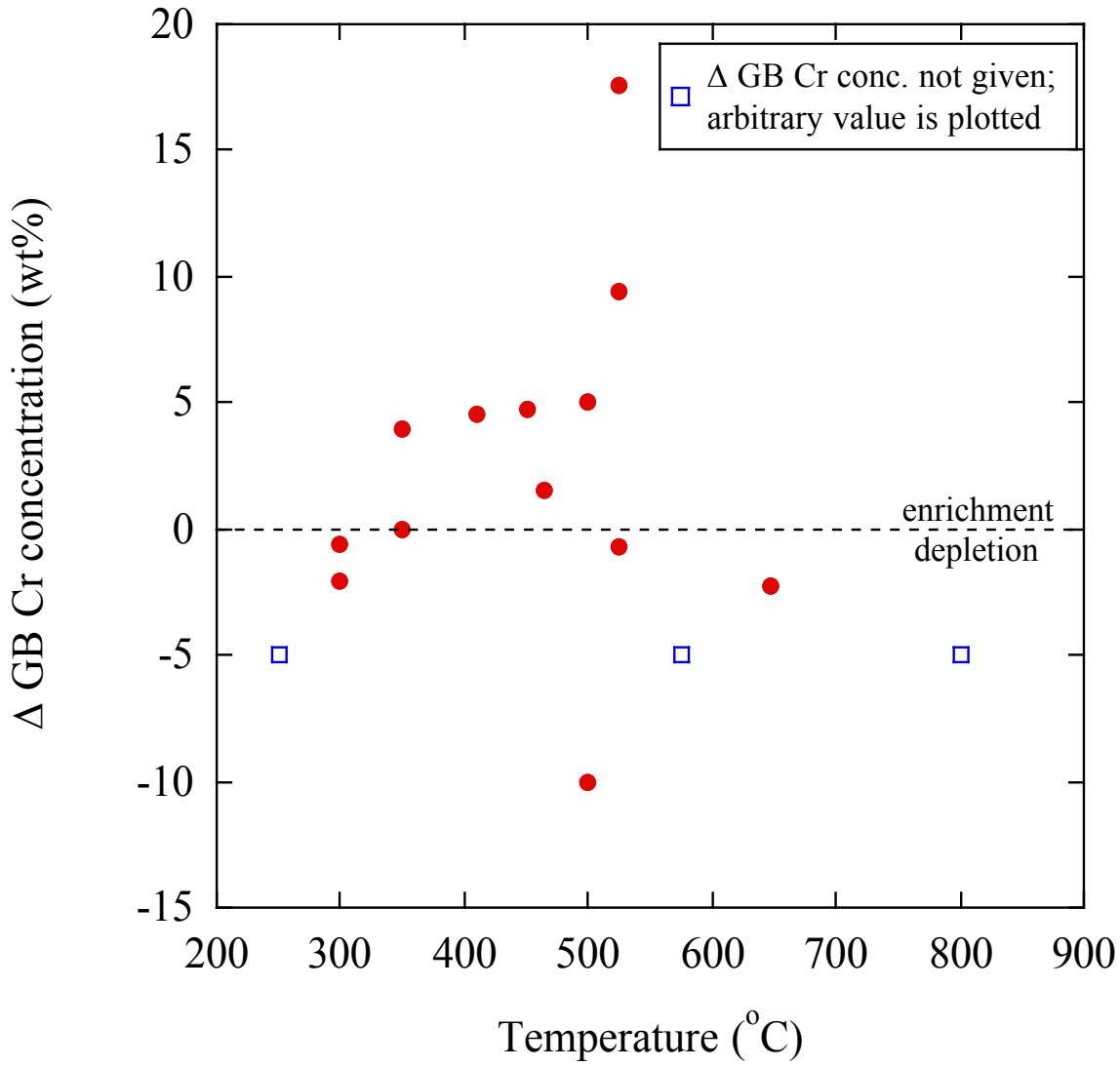

Figure 12. Temperature dependence of the change in grain boundary Cr concentration (wt%), from all experiments reported in literature except for electron irradiation experiments. The open squares represent studies in which the value of the change in grain boundary Cr concentration was not reported, thus an arbitrary value is plotted here simply to indicate the direction of RIS.

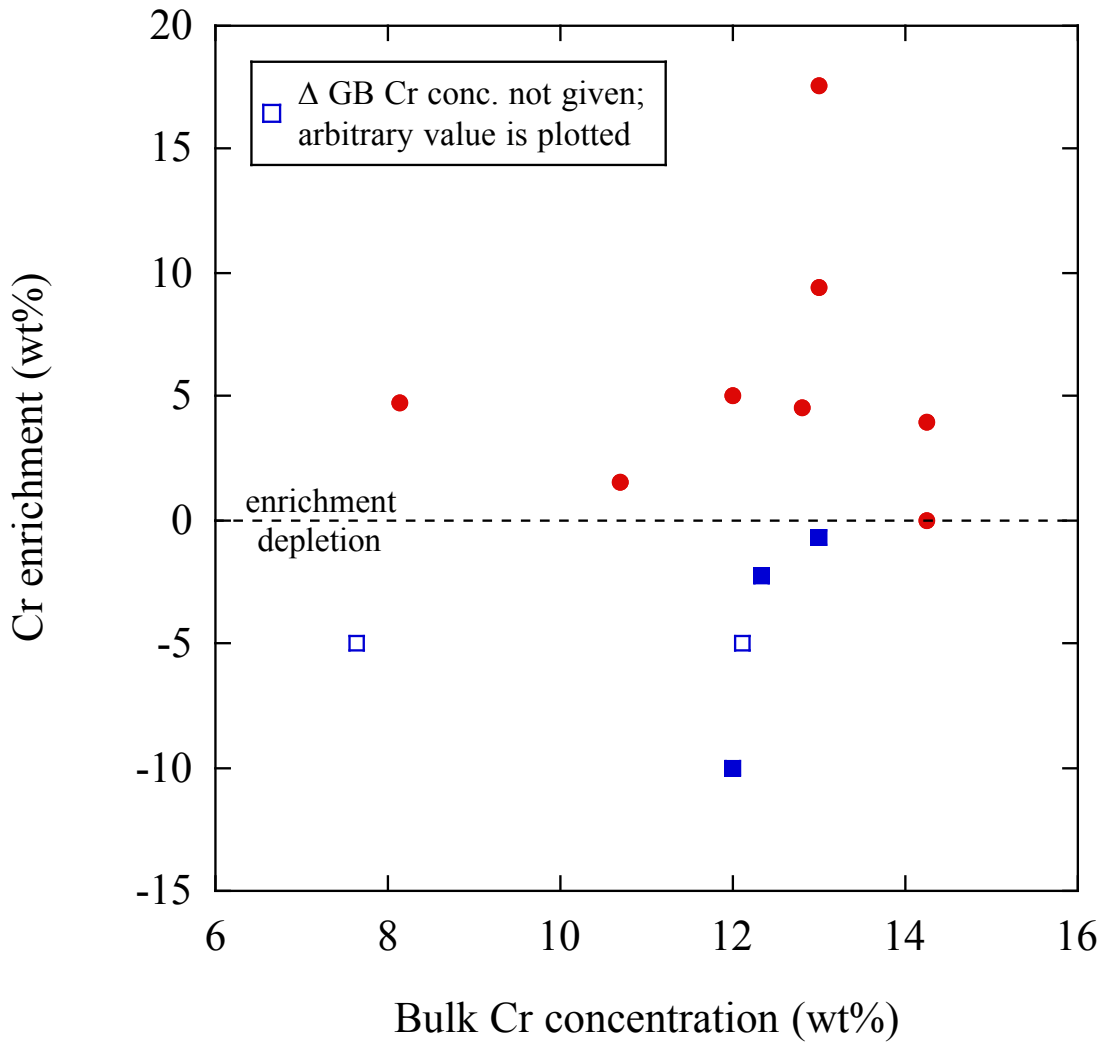

Figure 13. Bulk Cr concentration dependence of the change in grain boundary Cr concentration (wt%), from all experiments reported in literature except for electron irradiation and non-alloying element ion irradiation experiments. The open squares represent studies in which the value of the change in grain boundary Cr concentration was not reported, thus an arbitrary value is plotted here simply to indicate the direction of RIS.

References

[1] R. L. Klueh and D. R. Harries, *High-Chromium Ferritic and Martensitic Steels for Nuclear Applications*. ASTM, 2001.

[2] A. Kostka, K. Tak, R. Hellmig, Y. Estrin, and G. Eggeler, "On the contribution of carbides and micrograin boundaries to the creep strength of tempered martensite ferritic steels," *Acta Materialia*, vol. 55, no. 2, pp. 539–550, Jan. 2007.

[3] H. Takahashi, S. Ohnuki, and T. Takeyama, "Radiation-induced segregation at internal sinks in electron irradiated binary alloys," *Journal of Nuclear Materials*, vol. 103–104, pp. 1415–1420, 1981.

[4] T. Kato, H. Takahashi, S. Ohnuki, K. Nakata, and J. Kuniya, "The effect of solute content on grain boundary in electron-irradiated Fe-Cr-Mn alloys," *Journal of Nuclear Materials*, vol. 179–181, pp. 623–625, 1991.

[5] S. Ohnuki, H. Takahashi, and T. Takeyama, "Void swelling and segregation of solute in ion-irradiated ferritic steels," *Journal of Nuclear Materials*, vol. 103–104, pp. 1121–1125, 1981.

[6] R. E. Clausing, L. Heatherly, R. G. Faulkner, A. F. Rowcliffe, and K. Farrell, "Radiation-induced segregation in HT-9 martensitic steel," *Journal of Nuclear Materials*, vol. 141–143, pp. 978–981, 1986.

[7] E. A. Little, T. S. Morgan, and R. G. Faulkner, "Microchemistry of neutron irradiated 12%CrMoVNb martensitic steel," *Materials Science Forum*, vol. 97–99, pp. 323–328, 1992.

[8] Y. Hamaguchi, H. Kuwano, H. Kamide, R. Miura, and T. Yamada, "Effects of proton irradiation on the hardening behavior of HT-9 steel," *Journal of Nuclear Materials*, vol. 133–134, pp. 636–639, 1985.

[9] I. Neklyudov and V. Voyevodin, "Features of structure-phase transformations and segregation processes under irradiation of austenitic and ferritic-martensitic steels," *Journal of Nuclear Materials*, vol. 212–215, pp. 39–44, Sep. 1994.

[10] R. Schaeublin, P. Spatig, and M. Victoria, "Chemical segregation behavior of the low activation ferritic / martensitic steel F82H," *Journal of Nuclear Materials*, vol. 263, pp. 1350–1355, 1998.

[11] G. Gupta, Z. Jiao, A. N. Ham, J. T. Busby, and G. S. Was, "Microstructural evolution of proton irradiated T91," *Journal of Nuclear Materials*, vol. 351, no. 1–3, pp. 162–173, Jun. 2006.

[12] Z. Lu, R. Faulkner, N. Sakaguchi, H. Kinoshita, H. Takahashi, and P. Flewitt, "Effect of hafnium on radiation-induced inter-granular segregation in ferritic steel," *Journal of Nuclear Materials*, vol. 351, no. 1–3, pp. 155–161, Jun. 2006.

[13] E. A. Marquis, S. Lozano-Perez, and V. De Castro, "Effects of heavy-ion irradiation on the grain boundary chemistry of an oxide-dispersion strengthened Fe–12wt.% Cr alloy," *Journal of Nuclear Materials*, vol. 417, pp. 257–261, Oct. 2011.

[14] E. A. Marquis, R. Hu, and T. Rousseau, "A systematic approach for the study of radiation-induced segregation/depletion at grain boundaries in steels," *Journal of Nuclear Materials*, vol. 413, no. 1, pp. 1–4, Jun. 2011.

[15] Z. Lu, R. G. Faulkner, G. Was, and B. D. Wirth, "Irradiation-induced grain boundary chromium microchemistry in high alloy ferritic steels," *Scripta Materialia*, vol. 58, no. 10, pp. 878–881, May 2008.

[16] J. F. Ziegler, "The Stopping and Range of Ions in Matter (SRIM)," 2013.

[17] T. R. Allen, J. T. Busby, G. S. Was, and E. A. Kenik, "On the mechanism of radiation-induced segregation in austenitic Fe–Cr–Ni alloys," *Journal of Nuclear Materials*, vol. 255, pp. 44–58, 1998.

[18] J. M. Perks and S. M. Murphy, "Modelling the major element radiation-induced segregation in concentrated Fe-Cr-Ni alloys," in *Materials for Nuclear Reactor Core Applications, Vol. 1, Bristol, UK*, pp. 165–169.

[19] J. M. Perks, A. D. Marwick, and C. A. English, "A Computer Code to Calculate Radiation-Induced Segregation in Concentrated Ternary Alloys," *Materials Development Division, Harwell Laboratory, AERE-R 12121*.

[20] T. R. Allen and G. S. Was, "Modeling radiation-induced segregation in austenitic Fe–Cr–Ni alloys," *Acta Materialia*, vol. 46, no. 10, pp. 3679–3691, Jun. 1998.

[21] S. Choudhury et al., "Ab-initio based modeling of diffusion in dilute bcc Fe–Ni and Fe–Cr alloys and implications for radiation induced segregation," *Journal of Nuclear Materials*, vol. 411, no. 1–3, pp. 1–14, Apr. 2011.

[22] K. L. Wong, H.-J. Lee, J.-H. Shim, B. Sadigh, and B. D. Wirth, "Multiscale modeling of point defect interactions in Fe–Cr alloys," *Journal of Nuclear Materials*, vol. 386–388, pp. 227–230, Apr. 2009.

[23] K. Wong, J. Shim, and B. Wirth, "Molecular dynamics simulations of point defect interactions in Fe–Cr alloys," *Journal of Nuclear Materials*, vol. 367–370, pp. 276–281, Aug. 2007.

[24] P. Olsson, "Ab initio study of interstitial migration in Fe–Cr alloys," *Journal of Nuclear Materials*, vol. 386–388, pp. 86–89, Apr. 2009.

[25] P. Olsson, C. Domain, and J. Wallenius, "Ab initio study of Cr interactions with point defects in bcc Fe," *Physical Review B*, vol. 75, no. 1, pp. 1–12, Jan. 2007.

[26] J. P. Wharry and G. S. Was, "The mechanism of radiation-induced segregation in ferritic-martensitic alloys," *submitted*.

[27] D. Terentyev, P. Olsson, T. P. C. Klaver, and L. Malerba, "On the migration and trapping of single self-interstitial atoms in dilute and concentrated Fe–Cr alloys: Atomistic study and comparison with resistivity recovery experiments," *Computational Materials Science*, vol. 43, no. 4, pp. 1183–1192, Oct. 2008.

[28] C. R. Hubbard, H. E. Swanson, and F. A. Mauer, "A silicon powder diffraction standard reference material," *Journal of Applied Crystallography*, vol. 8, pp. 45–48, 1975.

[29] A. Taylor, "Lattice parameters of binary nickel-cobalt alloys," *Journal of the Institute of Metals*, vol. 77, pp. 585–594, 1950.

[30] M. E. Straumanis and L. S. Yu, "Lattice parameters, densities, expansion coefficients and perfection of structure of Cu and of Cu-In α phase," *Acta Crystallographica, Section A (Crystal Physics, Diffraction, Theoretical and General Crystallography)*, vol. A25, no. 6, pp. 676–682, 1969.

[31] R. G. Ross and W. Hume-Rothery, "High temperature x-ray metallography, I. A new Debye-Scherrer camera for use at very high temperatures, II. A new parafocusing camera, III. Applications to the study of chromium, hafnium, molybdenum, rhodium, ruthenium, and tungsten," *Journal of the Less-Common Metals*, vol. 5, no. 2, pp. 258–270, 1963.

[32] N. Schmitz-Pranghe and R. Kohlhaas, "X-ray diffraction investigation of liquid iron, cobalt and nickel," *Zeitschrift fur Naturforschung A (Astrophysik, Physik und Physikalische Chemie)*, vol. 25, no. 11, p. 1752, 1970.

[33] G. S. Was, *Fundamentals of Radiation Materials Science: Metals and Alloys*. Springer, 2007.